






Article

Complexes of Cobalt(II) Iodide with Pyridine and Redox Active 1,2-Bis(arylimino)acenaphthene: Synthesis, Structure, Electrochemical, and Single Ion Magnet Properties

Dmitriy S. Yambulatov ^{1,*}, Stanislav A. Nikolaevskii ^{1,*}, Mikhail A. Kiskin ¹,
Tatiana V. Magdesieva ², Oleg A. Levitskiy ², Denis V. Korchagin ³, Nikolay N. Efimov ¹,
Pavel N. Vasil'ev ¹, Alexander S. Goloveshkin ⁴, Alexey A. Sidorov ¹ and Igor L. Eremenko ^{1,4}

¹ N. S. Kurnakov Institute of General and Inorganic Chemistry, Russian Academy of Sciences, 31 Leninsky prosp., 119991 Moscow, Russian

² Lomonosov Moscow State University, Department of Chemistry, Leninskie Gory 1/3, 119991 Moscow, Russia

³ Institute of Problems of Chemical Physics, Russian Academy of Sciences, Chernogolovka, 142432 Moscow Region, Russia

⁴ Nesmeyanov Institute of Organoelement Compounds, 119991 Moscow, Russia

* Correspondence: yambulatov@yandex.ru (D.S.Y.); sanikol@igic.ras.ru (S.A.N.); Tel.: +7-495-955-4817 (S.A.N.)

Academic Editor: Constantina Papatriantafyllopoulou

Received: 18 March 2020; Accepted: 24 April 2020; Published: 28 April 2020



Abstract: Complexes [(dpp-BIAN)⁰Co^{II}I₂]·MeCN (**I**) and [(Py)₂CoI₂] (**II**) were synthesized by the reaction between cobalt(II) iodide and 1,2-bis(2,6-diisopropylphenylimino)acenaphthene (dpp-BIAN) or pyridine (Py), respectively. The molecular structures of the complexes were determined by X-ray diffraction. The Co(II) ions in both compounds are in a distorted tetrahedral environment (CoN₂I₂). The electrochemical behavior of complex **I** was studied by cyclic voltammetry. Magnetochemical measurements revealed that when an external magnetic field is applied, both compounds exhibit the properties of field-induced single ion magnets.

Keywords: cobalt(II) complexes; redox active ligand; cyclic voltammetry; single ion magnet; dpp-bian; acenaphthenediimine

1. Introduction

The activity in the research of mononuclear cobalt complexes with various types of donor ligands, which has been observed in the last decade, is explained by the orbital moment of the Co(II) ion as well as the spin-orbit coupling [1,2]. Both of these factors influence the possibility of splitting the term of the ground state of the complex in a zero field. Axial splitting in a zero field (D), which characterizes the magnetic anisotropy of the metal ion in the complex, is a necessary condition for the manifestation of the properties of a single molecule or single ion magnet (SIM). Creating conditions for a metal ion to manifest high magnetic anisotropy is a priority in the chemistry of complexes compared to additive schemes for increasing the total spin of the system. The anisotropy of the Co(II) ion can be controlled by rational selection of ligands with a set of finely tuned characteristics of the spatial and electronic structure. The use of spatially branched functional groups capable of defining unusual types of geometry of the Co(II) atom is effectively used in the design of SIMs. On the other hand, fine tuning of magnetic anisotropy can be carried out by varying the ligand field strength, which is usually achieved due to the optimal combination of the number and relative position of substituents of a different electronic nature. At the same time, the strategy of the controlled ligand field strength, based

on the use of redox-active molecules capable of reversibly and controllably changing their electronic characteristics while maintaining a high degree of structural rigidity, has been studied scarcely for the molecular design of SIM [3–5].

Redox-active ligands can form metal-radical complexes, interest in which is caused when solving problems of creating materials with tuned properties [6,7]. The generation/degradation of the radical in the composition of the complex can significantly affect the luminescent and magnetic properties, conductivity, catalytic activity, etc. [8–12].

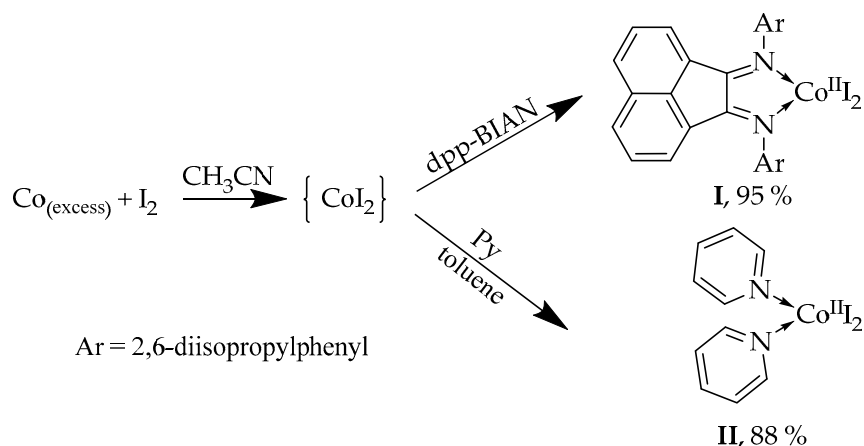
As the main object of our research, we selected a complex of cobalt(II) iodide with 1,2-bis(2,6-diisopropylphenylimino)acenaphthene (dpp-BIAN). The ligand dpp-BIAN is widely known for its unique ability to accept reversibly up to four electrons [13], which allows one to control the ligand field strength over a wide range. Moreover, the catalytic activity towards a number of industrially important reactions [14–17], visible light-harvesting behavior for potential photovoltaic applications [18,19], biological activity [20], as well as ability for small molecule activation [21] shown by transition metal complexes of neutral, mono-, and dianionic forms of dpp-BIAN could be finely tuned due to the unique redox features of this ligand [22–28]. On the other hand, the possibility of reversible generation of radical anions ($[(\text{dpp-BIAN})^0] \rightleftharpoons [(\text{dpp-BIAN})^-]$) may allow the exchange interactions of the ferromagnetic nature in the complex molecule to be switched on, which can also have an effect on the SIM magnetization reversal barrier. Iodide anions were selected as additional ligands due to data indicating the heavy atoms effect of halogens on the magnetic anisotropy of Co(II)-based SIMs [29].

As an additional object of research, we studied the complex of cobalt(II) iodide with pyridine. Despite their chemical simplicity, it is surprising that the coordination compounds of CoI_2 with substituted pyridine ligands have received scarce attention [30–36]. A comparison study of these two systems allowed us to draw preliminary conclusions about the potential use of redox-active ligands of the Ar-BIAN class in the Co(II)-SIM-directed design.

2. Results and Discussion

2.1. Synthesis and Characterization of $[(\text{dpp-BIAN})^0\text{Co}^{\text{II}}\text{I}_2] \cdot \text{MeCN}$ (I) and $[(\text{Py})_2\text{CoI}_2]$ (II)

The reaction between 1,2-bis[(2,6-diisopropylphenyl)imino]acenaphthene and cobalt diiodide in a solution of acetonitrile (Scheme 1) resulted in complex $[(\text{dpp-BIAN})^0\text{Co}^{\text{II}}\text{I}_2]$ (I). The reaction proceeded in an inert atmosphere on heating and was accompanied by a rapid change in the color of the solution from green to red-brown. The product crystallized at room temperature from the initial volume of solvent in high yield (95%). Due to the extreme hygroscopicity of cobalt iodide [37], it was synthesized in situ from crystalline iodine and an excess of metal cobalt. Preliminary data on the state of the redox-active ligand in I can be obtained from its IR spectrum by the presence of characteristic bands of stretching vibrations of the double bond $\text{C}=\text{N}$ ($1646\text{--}1600\text{ cm}^{-1}$) of neutral diimine dpp-BIAN [38,39] and the absence of absorption bands of the three-electron $\text{C}-\text{N}$ bonds ($1550\text{--}1500\text{ cm}^{-1}$) of the dpp-BIAN anion-radical and the $\text{C}-\text{N}$ bonds (1310 cm^{-1}) of the dianionic form of the ligand [40,41]. The synthesis of the cobalt(II) iodide complex with dpp-BIAN was first reported in an article on the polymerization of α -olefins [39], but its crystal structure was not described since single crystals were not isolated—the composition of the obtained compound was established by indirect methods. The synthesis and molecular structure of another congener $[(\text{mes-BIAN})^0\text{Co}^{\text{II}}\text{I}_2]$ (mes-BIAN = di-(2,4,6-trimethylphenyl)-bis-acenaphthenequinonediimine) was reported; however, their magnetic and redox properties were not discussed [42].



Scheme 1. Synthesis of complexes **I** and **II**.

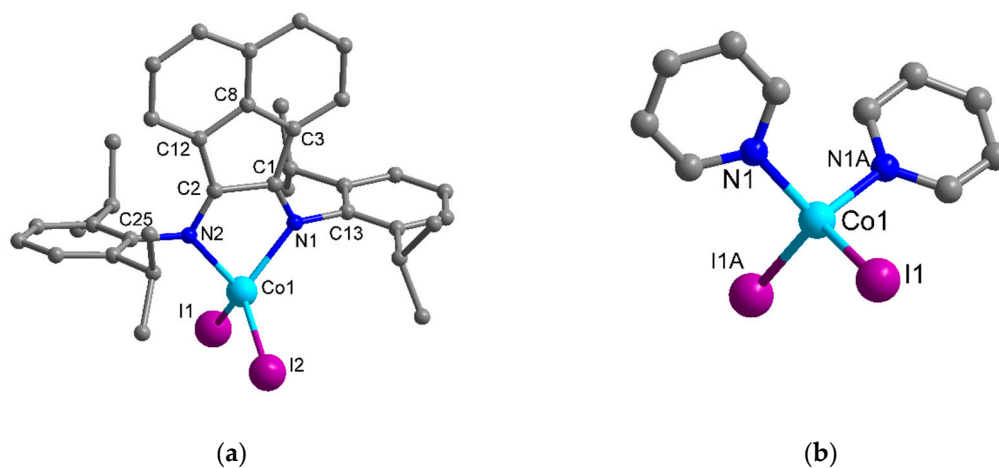
When pyridine was allowed to react with cobalt(II) iodide in a 2:1 molar ratio in toluene (Scheme 1), complex $[(\text{Py})_2\text{CoI}_2]$ (**II**) was isolated. Dry CoI_2 was used for the synthesis (see the experimental part), in which a toluene medium reacted heterogeneously with two equivalents of pyridine. Single crystals suitable for X-ray diffraction were grown by slowly ($10\text{ }^\circ\text{C}$ per hour) cooling the reaction mixture from 130 to $25\text{ }^\circ\text{C}$ and then keeping it for 2 h. For the first time, the synthesis of the complex of cobalt diiodide with pyridine was described as early as 1927 [43]; the authors described the color of the compound (blue) and performed elemental analysis of the iodine content. In 1978, Bill Little et al. [44] described the synthesis of the compound of the composition $[(\text{Py})_2\text{CoI}_2]$ and characterized it by powder X-ray diffraction. Thus, single crystal X-ray diffraction studies for compound **II** were performed here for the first time. The powder X-ray diffraction pattern of the compound prepared here (Figures S1, S2, see Supplementary Material) differs from the powder X-ray diffraction pattern reported [44] (Table S1, see Supplementary Material). No similarity of interplanar distances was observed, which allows us to conclude that, apparently, in this work, we obtained another compound or another polymorphic modification of $[(\text{Py})_2\text{CoI}_2]$.

2.2. Molecular Structures

Complexes **I** and **II** crystallized in the orthorhombic space groups $Pbca$ and $Pbcn$, respectively; the crystal and experiment data are listed in Table 1. The crystal of complex **I** is solvate with one molecule of MeCN. Both compounds are mononuclear, in which the cobalt(II) ion coordinates two I^- anions and two N atoms of chelate ligand dpp-BIAN (**I**, Figure 1a) or two monodentate ligands Py (**II**, Figure 1b). In crystal **II**, the second-order axis C_2 passes through the metal atom between pairs of atoms I and N. For complex **I**, the N-Co-N angle ($81.24(12)^\circ$) is much smaller than the others (N-Co-I $112.49(9)$ – $117.61(9)^\circ$, I-Co-I $109.33(2)^\circ$) due to the chelating nature of the ligand (Co-N $2.073(3)$, $2.090(3)$ Å, Co-I $2.5343(7)$, $2.5346(6)$ Å). In **II**, the I-Co-I angle ($115.80(7)^\circ$) is larger, while the N-Co-I ($108.0(2)^\circ$, $109.0(2)^\circ$) and N-Co-N ($106.7(4)^\circ$) angles are close to the angle for a perfect tetrahedron. The Co-N bond length ($2.041(7)$ Å) in **II** decreased by ~ 0.04 Å as compared to **I**, while the Co-I bond ($2.5643(11)$ Å) increased by ~ 0.03 Å. The observed bond lengths are comparable with the known values for complexes with a similar coordination environment of CoN_2I_2 [29,32,35,36,39,45,46]. The deviation of the angular geometry of the polyhedra from the ideal tetrahedron was estimated by calculating the parameter $\delta = 2T_d - (\alpha + \beta)$, where angles $\alpha = \text{N-Co-N}$, $\beta = \text{I-Co-I}$, and $T_d = 109.5^\circ$. Based on the calculations, the coordination environment of CoN_2I_2 in **I** corresponds to a compressed pseudotetrahedron ($\delta = 28.43$), while that in **II** corresponds to a tetrahedron ($\delta = -3.5$).

Table 1. Crystallographic data, details of the data collection, and characteristics of the data refinement for I and II.

Parameter	Value	
	I	II
Molecular formula	C ₃₈ H ₄₃ CoI ₂ N ₃	C ₁₀ H ₁₀ CoI ₂ N ₂
<i>M</i> _w	854.48	470.93
<i>T</i> , K		296(2)
Crystal system		Orthorhombic
Space group	<i>Pbca</i>	<i>Pbcn</i>
<i>a</i> , Å	19.5759(4)	13.488(2)
<i>b</i> , Å	19.3545(4)	7.1497(10)
<i>c</i> , Å	19.7703(5)	14.588(2)
<i>V</i> , Å ³	7490.6(3)	1406.7(3)
<i>Z</i>	8	4
ρ _{calcd} , g cm ⁻³	1.515	2.224
μ, mm ⁻¹	2.135	5.582
θ range, deg	2.06–28.28	2.79–30.59
<i>F</i> (000)	3400	868
Index range	−26 ≤ <i>h</i> ≤ 25; −25 ≤ <i>k</i> ≤ 25; −26 ≤ <i>l</i> ≤ 25	−19 ≤ <i>h</i> ≤ 19; −10 ≤ <i>k</i> ≤ 10; −20 ≤ <i>l</i> ≤ 20
Number of reflections collected	75256	15566
Number of unique reflections	9291	2160
<i>R</i> _{int}	0.099	0.162
Number of reflections with <i>I</i> > 2σ(<i>I</i>)	6692	1030
<i>Goof</i>	1.051	1.000
<i>R</i> factor on <i>F</i> ² > 2σ(<i>F</i> ²)	<i>R</i> ₁ = 0.062, <i>wR</i> ₂ = 0.140	<i>R</i> ₁ = 0.074, <i>wR</i> ₂ = 0.148
<i>R</i> factor (all data)	<i>R</i> ₁ = 0.091, <i>wR</i> ₂ = 0.155	<i>R</i> ₁ = 0.157, <i>wR</i> ₂ = 0.182
Δρ _{max} /Δρ _{min} , e/Å ³	−1.113/0.837	−1.135/0.966

**Figure 1.** Molecular structure of complexes I (a) and II (b). Hydrogen atoms are omitted. Symmetry codes used to generate equivalent atoms for II: (A) $-x + 1, y, -z + 1/2$.

The C–C and C–N bond lengths in the α -diimine fragment of complex I (C(1)–C(2) 1.515(5) Å, C(1)–N(1) 1.276(5) Å, C(2)–N(2) 1.280(5) Å) as compared to dpp-BIAN (C–C 1.527 Å, C–N 1.272, 1.272 Å) [47] as well as cobalt(II) [(dpp-BIAN)⁰Co^{II}Cl₂] (C–C 1.564 Å, C–N 1.231, 1.286 Å) [39,48], [(dpp-BIAN)⁰Co^{II}Br₂] (C–C 1.531 Å, C–N 1.268, 1.286 Å) [49], and iron(II) [(dpp-BIAN)⁰Fe^{II}Br₂] complexes (C–C 1.508 Å, C–N 1.277, 1.287 Å) [50], [(dpp-BIAN)⁰Fe^{II}Cl₂] (C–C 1.506 Å, C–N 1.288, 1.271 Å) [51] indicate the neutral form of the ligand.

In **I**, π - π interactions were observed between the benzene rings of the acenaphthene fragment (the shortest C...C distance is 3.308(6) Å), the interatomic distance between nearby Co atoms is 9.7904(2) Å. In the crystal of molecule **II**, π - π interaction was observed between parallel pyridine ligands of neighboring complex molecules (the shortest C...C distance is 3.522(14) Å); the minimum interatomic Co...Co distance is 7.6327(9) Å. An increase in the organic component decreases the calculated crystal density from 2.224 (**II**) to 1.515 g/cm³ (**I**).

2.3. Solid State Magnetic Susceptibilities

The temperature dependences of the magnetic susceptibility of complexes **I** and **II** were studied in the range of 2–300 K in a magnetic field of 5 kOe (Figure 2). The $\chi_m T$ values of both complexes at 300 K (2.93 and 2.48 cm³ mol⁻¹ K for **I** and **II**, respectively) are significantly higher than the pure spin value (1.88 cm³ mol⁻¹ K) [52], which may indicate a significant orbital contribution to the total magnetic moment. The $\chi_m T$ dependence remains almost linear to 100 K; with a further decrease in temperature, the $\chi_m T$ values gradually decrease and reach a minimum at $T = 2$ K (1.63 and 1.24 cm³ mol⁻¹ K for **I** and **II**, respectively). Such behavior may be due to significant magnetic anisotropy, and/or the Zeeman effect (saturation effect) when an external magnetic field is applied.

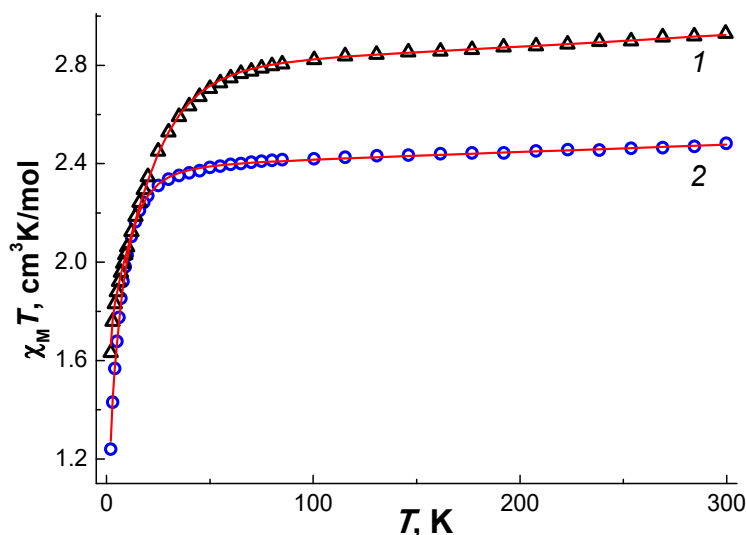


Figure 2. Temperature dependences $\chi_m T$ of complexes **I** (1) and **II** (2) ($H = 5$ kOe). Lines are the result of approximation of experimental data with Equation (1) (see text).

The χT curves were approximated using spin Hamiltonian (Equation (1)):

$$\hat{H} = D \left[\hat{S}_Z^2 - \frac{1}{3} S(S+1) \right] + \mu_B (B_X g_X \hat{S}_X + B_Y g_Y \hat{S}_Y + B_Z g_Z \hat{S}_Z) \quad (1)$$

where $S = 3/2$ is the spin of the high-spin Co(II) ion, D is the axial ZFS parameter, and g_α ($\alpha = X, Y, Z$) are the principle values of the g -tensor; μ_B is the Bohr magneton; and $g_x, g_y,$ and g_z are the components of the g -tensor using the PHI program [53]. An analysis of the approximation results revealed the presence of an excessive number of parameters in the case of an anisotropic g -tensor; therefore, the case of an isotropic g -tensor ($g_x = g_y = g_z = g_{iso}$) was used. Our calculations (see Table 2) showed that the curves can be described by both negative and positive parameters D . Nonzero absolute values of D indicate the presence of magnetic anisotropy of the cobalt(II) ion. A nonzero negative value of the parameter zJ' for **II** indicates the presence of weak intermolecular interactions between metal ions, which correlates with the X-ray diffraction data.

Table 2. Scalar D - and g -tensor parameters fitted with Equation (1) and CASSCF/NEVPT2 calculation for **I** and **II**.

Complex/ Parameter	Best-Fit Parameters with Equation (1)			CASSCF/NEVPT2 Calculation		
	D, cm^{-1}	g_{iso}	zJ, cm^{-1}	D, cm^{-1}	E/D	g
I [2 ex]	−25.7(3)	2.481(1)	0	−22.6	0.294	$g_x = 2.251$
	24.6(3)	2.481(1)	0			$g_y = 2.331$ $g_z = 2.515$ ($g_{\text{iso}} = 2.366$)
II [2 ex]	−8.2(2)	2.285(1)	−0.07(1)	−5.9	0.094	$g_x = 2.248$
	7.6(2)	2.287(1)	−0.09(1)			$g_y = 2.272$ $g_z = 2.333$ ($g_{\text{iso}} = 2.284$)

CASSCF/NEVPT2 calculations allowed this ambiguity to be passed by determination of the zero-filed splitting parameters for cobalt(II) ions in **I** and **II**. The calculated principle values of the D - and g -tensors for **I** and **II** are listed in Table 2, where all the calculated D values are negative, and the D and g_{iso} values are all close to the values calculated for the experimental magnetic data. The negative values of the ZFS parameters suppose easy-axis magnetic anisotropy and the probability of realizing SIM properties (out-of-phase AC susceptibility signals and slow magnetic relaxation) [29,54].

Table 3 displays the energy levels (cm^{-1}) for **I** and **II** calculated from spin Hamiltonian (1) and CASSCF/NEVPT2 (in zero-filed and applied field). The energy values fitted and calculated from CASSCF/NEVPT2 are in good agreement.

Table 3. Energy levels (cm^{-1}) for **I** and **II** from Hamiltonian (1) approximation of the temperature dependences and CASSCF/NEVPT2 calculations.

State	M_s	I (calc)	I ($H_{\text{DC}} = 0$ Oe)	I ($H_{\text{DC}} = 1.5$ kOe)	II (calc)	II ($H_{\text{DC}} = 0$ Oe)	II ($H_{\text{DC}} = 2.5$ kOe)
1	−3/2	0	0	0	0	0	0
2	+3/2	0	0	0.53	0	0	0.92
3	−1/2	50.58	51.4	51.58	11.98	16.40	16.67
4	+1/2	50.58	51.4	51.75	11.98	16.40	16.94

In order to identify SIM behavior, measurements of the AC magnetic susceptibility were performed. The out-of-phase signal χ'' close to zero was observed in the absence of the DC-magnetic field for both complexes. An external DC-magnetic field H_{dc} application made it possible to detect distinct maxima on the χ'' values at 2 K in both cases. The optimal values of H_{dc} (1.5 and 2.5 kOe for **I**·MeCN and **II**, respectively) were obtained by the AC susceptibility measurements at various DC field strengths (Figures S3 and S4, see Supplementary Material).

The AC susceptibility data in the optimal DC field were fitted by the generalized Debye model (Figure 3), which allows determination of the relaxation time temperature dependencies of the magnetization (Figure 4). We tried to fit the $\tau(1/T)$ by the different relaxation mechanisms in order to better understand the relaxation pathways' nature [55,56]. As we can conclude from this experiment, the best agreement between the experimental data and theoretical dependences was achieved using the sum of Raman ($\tau_{\text{Raman}}^{-1} = C_{\text{Raman}} T^{n_{\text{Raman}}}$) and direct ($\tau_{\text{direct}}^{-1} = A_{\text{direct}} H^4 T$) relaxation mechanisms for both complexes (Figure 4, and Supplementary Material) with the best-fit parameters: $A_{\text{direct}} = 7.4$ and $7.5 \cdot 10^{-11} \text{ K}^{-1} \text{Oe}^{-4} \text{s}^{-1}$, $C_{\text{Raman}} = 0.46$, and $12 \text{ s}^{-1} \text{ K}^{-n_{\text{Raman}}}$, $n_{\text{Raman}} = 9.2$ and 9.4 for **I** and **II**, respectively.

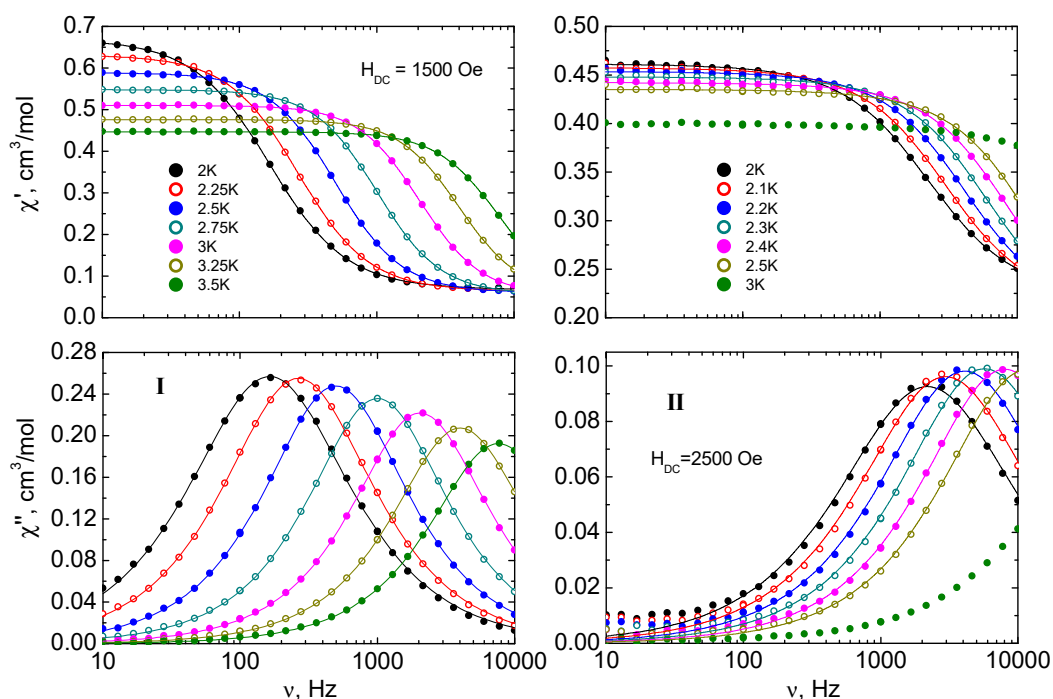


Figure 3. Frequency dependences of the real (χ' , top) and imaginary (χ'' , bottom) parts of the AC magnetic susceptibility at different temperatures for complexes I (left, $H = 1.5$ kOe, $T = 2$ – 3.5 K) and II (right, $H = 2.5$ kOe, $T = 2$ – 3 K). Lines show approximations of the data by the generalized Debye model.

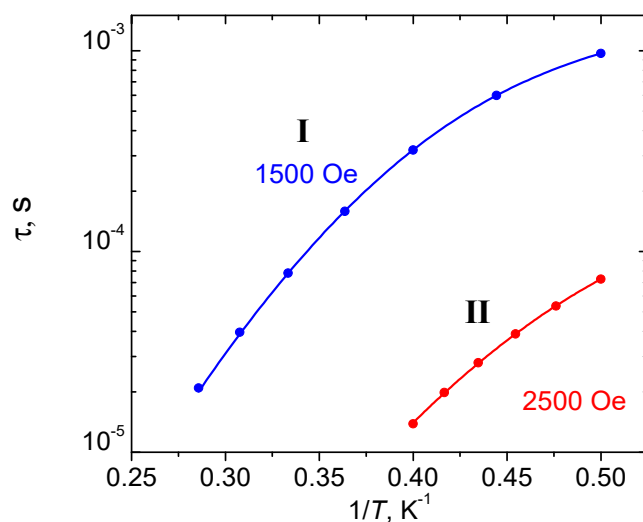


Figure 4. Dependence of the relaxation time τ on the reciprocal temperature for II ($H = 2.5$ kOe, $T = 2$ – 2.5 K). Lines show approximations of the curves by the sum of the Raman and direct relaxation mechanisms (blue solid line).

The fitting of the field dependences of the relaxation time as well as the negligible out-of-phase susceptibility in a zero field gives clear evidence of some additional temperature-independent relaxation pathways, presumably, the quantum tunneling, which suppress slow magnetic relaxation (see Supplementary Material). The data fit with use of the quantum tunneling ($\tau_{\text{QTM}}^{-1} = B_1/(1+B_2H^2)$) as an additional relaxation mechanism leads to overparameterization and mutual dependencies of the fit parameters.

It should be noted that the amplitude of the signal $\chi''(\nu)$ for complex II in the optimal field (Figure 3) increases with the temperature, which may be due to intermolecular or dipole–dipole interactions present in this compound. A similar behavior was previously observed for cobalt complexes [57], as

well as for other anisotropic ions, in particular, lanthanide ions [34,58–60]. For complex I, this behavior was not observed, which may be due to the large distance between metal ions in the crystal lattice.

A comparative analysis of the properties of I and similar complexes with chelate ligands (2,2'-biquinoline (biq) [34], 4,7-diphenyl-2,9-dimethyl-1,10-phenanthroline (bcp) [35], and 2,9-dimethyl-1,10-phenanthroline (dmphen) [36]) showed that the value of the parameter D can be both positive (10.3 cm^{-1} for $[\text{CoI}_2(\text{biq})]$ and 16.6 cm^{-1} for $[\text{CoI}_2(\text{dmphen})]$) and negative (-7.03 cm^{-1} for $[\text{CoI}_2(\text{bcp})]$).

Complex II can be compared with analog $[\text{CoI}_2(\text{quinoline})_2]$ [29], for which $D = 9.2\text{ cm}^{-1}$ and there is no slow magnetic relaxation. So, the nature of pyridine ligand changes the electronic structure of cobalt(II) ions, and this fine chemical tuning results in a switch of the magnetic behavior at low temperatures.

2.4. Cyclic voltammetry of $[(\text{dpp-BIAN})^0\text{Co}^{\text{II}}\text{I}_2]\cdot\text{MeCN}$ (I)

The electrochemical behavior of complex I was studied in solution; voltammograms were recorded for 2.1 M solutions of I in a 0.05 M solution of $n\text{-Bu}_4\text{NBF}_4$ in acetonitrile on a platinum disk working electrode (Figure 5).

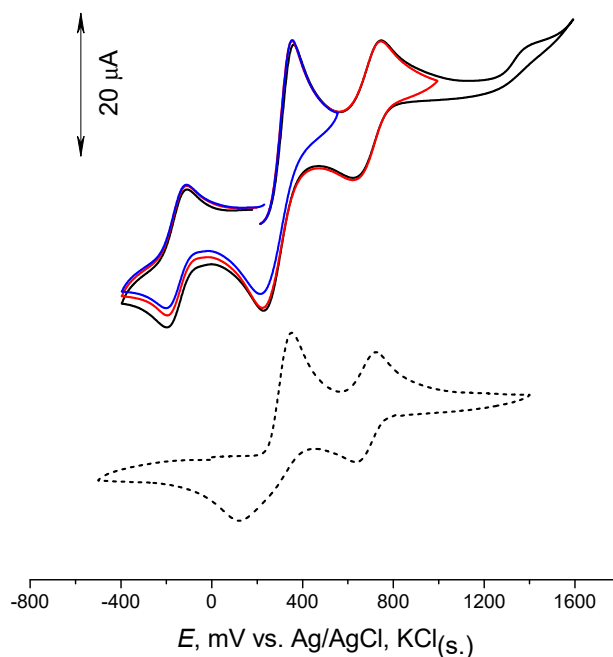
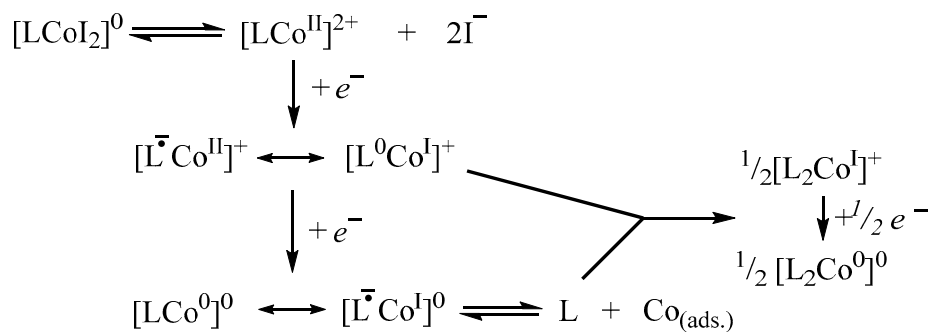


Figure 5. Voltammogram of I (solid lines, 2.1 mM at 0.05 M $n\text{-Bu}_4\text{NBF}_4$ in MeCN, 50 mV/s, Pt) and Bu_4NI (dashed line).

When dissolved in acetonitrile, both iodine atoms at the cobalt atom are replaced by solvate acetonitrile molecules. This follows from the analysis of the voltammograms with a potential sweep into the anode region (Figure 5): The first two anode processes correspond to the oxidation of free iodide ions (I^-/I_3^- and I_3^-/I_2 at potentials $E_{\text{pa}} = 0.36\text{ V}$ and 0.75 V , respectively). This is followed by an irreversible redox transition ($E_{\text{pa}} = 1.39\text{ V}$ at 50 mV/s), which corresponds to the oxidation of the ligand in the complex. This was concluded based on a comparison with the literature data for the imine oxidation potentials. The imine oxidation is irreversible and is observed in the range 1.5–1.7 V: For example, for PhCH=NPh , the oxidation potential is 1.59 V (vs SCE, Pt, MeCN [61]); and for free dpp-BIAN, the oxidation potential is 1.02 V (Pt, THF, vs. $\text{Fc}^{+/0}$ when converted into Ag/AgCl , KCl_{sat} , this is 1.47 V [62]).

In the cathode potential region, a quasi-reversible redox transition I was observed with the structure of $[\text{L}^0\text{Co}^{\text{I}}]^+$ to the electronic structure of the reduced complex (Scheme 2).



Scheme 2. Cathodic transformations of complex I.

At a potential of -0.68 V, a cathodic peak **II** was observed accompanied by the destruction of the complex with the deposition of cobalt on the electrode surface, which can be seen from the appearance of the oxidation peak of cobalt deposited on the backward curve ($E_{\text{pa}} = +0.13$ V) [63]. This cathodic process proceeds electrochemically slowly, which manifests itself in a very flat peak shape ($E_p - E_{p/2} = 93$ mV). In addition, analysis of the semi-integrated form of the voltammogram indicates that approximately half of the total amount of the complex is reduced (Figure 6b). It seems that free dpp-BIAN released upon cathodic destruction binds $[\text{L}^0\text{CoI}]^+$ to form a new complex $[\text{L}_2^0\text{CoI}]^+$. It contains a greater number of donor ligands than the original, which complicates its reduction. It is observed only when potential $E_{1/2} = -1.11$ V (peak **III**), which is substantially more anodic than the reduction potential of free ligand dpp-BIAN (-1.56 V [64]), which confirms the assignment of this redox transition. The limiting value of the half-integral function for the first cathode transition is equal to the sum for the second and third ones, which corresponds to the stoichiometry proposed in Scheme 2.

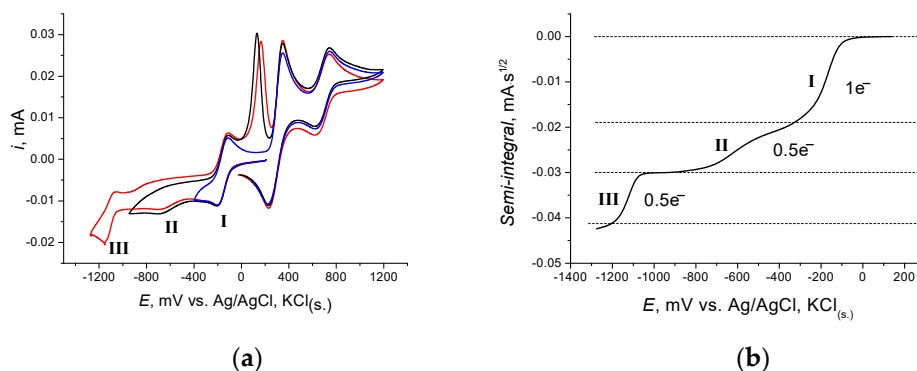


Figure 6. (a) Voltammogram of **I** (2.1 mM in 0.05 M $n\text{-Bu}_4\text{NBF}_4$ in MeCN, 50 mV/s, Pt); (b) semi-integral transformation of the cathode part of the voltammogram shown in Figure 6a.

3. Materials and Methods

3.1. General Remarks

Initial cobalt(II) iodide is sensitive to air moisture (it forms crystalline hydrates); therefore, all synthetic procedures and the isolation of reaction products were performed in an inert atmosphere using the Schlenk technique. Acetonitrile was dried over phosphorus(V) oxide and stored over molecular sieves (3 Å), toluene was dried and stored over the sodium complex with benzophenone, and the solvents were taken using condensation in vacuum immediately before use. Cobalt(II) iodide was synthesized *in situ* from metallic cobalt and crystalline iodine (Merck KGaA, Darmstadt, Germany) in acetonitrile in a glass ampoule with a Teflon valve under heating; dpp-BIAN was synthesized according to the known procedure [38]; and pyridine (Merck KGaA, Darmstadt, Germany) was dried over potassium hydroxide, stored over activated molecular sieves (4 Å), and condensed in vacuum

immediately before the reaction. Product yields were calculated relative to the initial amount of ligands: dpp-BIAN (0.50 g, 1 mmol) and pyridine (0.158 g, 2 mmol).

IR spectra of the compound were recorded in the range 400–4000 cm^{-1} on a Perkin Elmer (Waltham, Massachusetts, USA) Spectrum 65 spectrophotometer equipped with Quest ATR Accessory (Specac (Orpington, Kent, UK)) using the method of attenuated total reflection (ATR).

Voltammograms of the complexes were recorded on an AutoLab PGSTAT100 N (Metrohm, Zurich, Switzerland) potentiostat in a 10-mL three-electrode cell with a platinum wire counter electrode and a silver reference electrode (Ag/AgCl, KCl_{sat}). A reference electrode was attached to the electrolyte solution through a salt bridge containing a 0.05 M solution of *n*-Bu₄NBF₄ in acetonitrile. A platinum disk with an active surface area of 0.045 cm^2 was used as a working electrode. The platinum electrode was polished with a suspension of Al₂O₃ (SPA 0.3) at a polishing set (Metrohm, Zurich, Switzerland) and washed with sulfuric acid and water with acetone. All solutions were thoroughly deaerated with argon. A solution of complex **I** was prepared in acetonitrile in a Schlenk vessel in an argon atmosphere.

The magnetic behavior of the complexes was studied using the automated Quantum Design PPMS-9 physical property measuring system with the option of measuring the dynamic (AC) and static (DC) magnetic susceptibility. This equipment allows research to be carried out in the temperature range of 2–300 K with magnetic fields from −9 to 9 T. When measuring the AC susceptibility, an alternating magnetic field was applied with intensity $H_{\text{AC}} = 1\text{--}5$ Oe in the frequency range 10–10000 Hz. The measurements were carried out on polycrystalline samples moistened with mineral oil to prevent the orientation of the crystals in an external magnetic field. The prepared samples were sealed in plastic bags. The magnetic susceptibility χ was determined taking into account the diamagnetic contribution of the substance, using the additive Pascal scheme, the contribution of the bag, and that of mineral oil. The magnetization relaxation times $\tau = 1/2\pi\nu_{\text{max}}$ and the α factor that determines the distribution of relaxation processes were calculated by approximating the dependences $\chi'(\nu)$ and $\chi''(\nu)$ by the generalized Debye model.

Elemental analysis was performed on an automatic EuroEA-3000 C, H, N, S analyzer (EuroVektor, Pavia, Italy).

X-ray powder diffraction studies were carried out on a Bruker D8 Advance powder X-ray diffractometer (Bruker AXS, Madison, Wisconsin) equipped with variable slots, an Ni filter, and a LynxEye position-sensitive detector. The survey was carried out in the X-ray reflection mode (Bragg-Brentano geometry) with rotation of the sample. The diffraction pattern was described by the Rietveld method in the TOPAS software package.

X-ray diffraction studies of single crystals of complexes **I** and **II** were performed on a Bruker Apex II diffractometer (Bruker AXS, Madison, Wisconsin) (CCD detector, MoK $_{\alpha}$, $\lambda = 0.71073$ Å, graphite monochromator) [65]. The structures were solved by direct methods and refined in the full-matrix anisotropic approximation for all non-hydrogen atoms. Hydrogen atoms at carbon atoms of organic ligands were generated geometrically and refined in the "riding" model. The calculations were performed using the SHELX-2014 software package [66]. The main crystallographic parameters and refinement details of compounds **I** and **II** are listed in Table 1. The structure parameters were deposited with the Cambridge Structural Database (CCDC Nos. 1961151 (**I**) and 1961152 (**II**); deposit@ccdc.cam.ac.uk or http://www.ccdc.cam.ac.uk/data_request/cif).

Quantum chemical calculations of the zero-field splitting (ZFS) parameters for complexes **I** and **II** were performed based on the state-averaged complete active space self-consistent field calculations (SA-CASSCF) [67–69], followed by the N-electron valence second-order perturbation theory (NEVPT2) [70,71]. Scalar relativistic effects were taken into account by a standard second-order Douglas–Kroll–Hess (DKH) procedure [72]. For the calculations, a segmented all-electron relativistically contracted version [73] of Ahlrichs polarized triple- ζ basis set def2-TZVP [74–76] was used for all atoms. In order to decrease the calculation time, the resolution of identity (RI) approximation with corresponding correlation fitting of the basis set [77] was employed. The spin-orbit effects were included using the quasi-degenerate perturbation theory (QDPT) [78] in which approximations to

the Breit–Pauli form of the spin–orbit coupling operator (SOMF approximation) [79] and the effective Hamiltonian theory [80] were utilized. The CASSCF active space is defined by considering the seven d-electrons (for Co^{II}) distributed in the five 3d orbitals. All possible multiplet (10 quartet and 40 doublet) states arising from the d⁷ configuration were included into the wave function expansion. All quantum chemical calculations were performed by the ORCA program (ver.4.2.0) [81].

3.2. Synthesis of [(dpp-BIAN)⁰Co^{II}I₂]-MeCN (I)

Ligand dpp-BIAN (0.5 g, 1 mmol) was added to cobalt diiodide (1 mmol) prepared *in situ* in acetonitrile from iodine (0.254 g, 1 mmol) and an excess of powder metal cobalt. The color of the reaction mixture instantly changed from green to red-brown. Crystallization from acetonitrile gave red crystals in the form of parallelepipeds. Yield, 0.813 g (95%). Anal. calcd. for C₃₈H₄₃CoI₂N₃ (%): C, 53.41; H, 5.07; N, 4.92. Found (%): C, 53.35; H, 4.93; N, 4.87. IR (ATR, ν , cm⁻¹): 3063 w, 2961 s, 2925m, 2865m, 2249w, 1646m, 1620s, 1600m, 1583s, 1489w, 1462s, 1436s, 1420m, 1383m, 1364m, 1323m, 1291s, 1253m, 1222m, 1203w, 1188m, 1128m, 1112w, 1089w, 1052m, 1042m, 953m, 936m, 852w, 833s, 800vs, 779vs, 757vs, 738m, 611w, 587w, 541s, 515w, 468m, 436w.

3.3. Synthesis of [(Py)₂CoI₂] (II)

Cobalt diiodide (1 mmol) was synthesized *in situ* from crystalline iodine (0.254 g, 1 mmol) and an excess of powder metal cobalt in acetonitrile. Acetonitrile was removed from the [CoI₂ · xMeCN] adduct by drying in dynamic vacuum at 120 °C for 3 h. Toluene (25 mL) was condensed into a vial with CoI₂; then, pyridine (0.158 g, 2 mmol) was added, and the vial was sealed and heated in an oil bath at 130 °C until CoI₂ was completely dissolved. The color of the reaction mixture was blue. Slow cooling (10 °C per h) led to the formation of blue needle-shaped single crystals suitable for X-ray diffraction. Yield, 0.415 g (88%). Anal. calcd. for C₁₀H₁₀CoI₂N₂ (%): C, 25.50; H, 2.14; N, 5.95. Found (%): C, 25.28; H, 2.08; N, 5.74. IR (ATR, ν , cm⁻¹): 3058w, 1859w, 1660w, 1604vs, 1482m, 1442vs, 1352w, 1241w, 1208s, 1154w, 1061vs, 1044m, 1014m, 945w, 756vs, 691vs, 642vs, 446w, 426s, 416w.

4. Conclusions

Thus, here we presented the synthesis, characterization, and structures of two molecular complexes [(dpp-BIAN)⁰Co^{II}I₂]-MeCN (I) and [(Py)₂CoI₂] (II). The electrochemical studies of I suggest one-electron reduction of the ligand in the composition of the complex to a radical, which is useful for further study of its magnetic characteristics. The results of the DC magnetic measurements as well as CASSCF/NEVPT2 calculations showed that the distortion of the coordination CoN₂I₂ environment results in a negative axial magnetic anisotropy decrease from II ($D = -5.9$ cm⁻¹) to I ($D = -22.6$ cm⁻¹). According to the AC magnetometry, the complexes studied exhibit superparamagnetism and slow magnetic relaxation in the applied field H_{DC} , which classifies these compounds as field-induced SIMs. By the precise fit of the relaxation time dependencies it was shown that the main pathways of relaxation are Raman and direct, which is in common with other reported tetrahedral Co(II) SIMs.

Supplementary Materials: The following are available online at <http://www.mdpi.com/1420-3049/25/9/2054/s1>, Figures S1 and S2: Theoretical and experimental X-ray powder diffraction patterns of complexes I and II; Figures S3 and S4: Frequency dependences of the real (χ') and imaginary (χ'') parts of the dynamic magnetic susceptibility at different applied magnetic fields for complexes I and II; Table S1: Comparison of the position of the peaks in X-ray powder diffraction patterns with literature data for complex II. The relaxation time temperature dependencies fitted by using different mechanisms.

Author Contributions: D.S.Y. synthesized tested compounds; design of the study, D.S.Y., S.A.N., M.A.K.; manuscript writing, review and editing, D.S.Y., S.A.N., M.A.K., T.V.M., D.V.K., N.N.E., A.A.S., I.L.E.; X-Ray analysis M.A.K.; electrochemical analysis O.A.L. and T.V.M.; magnetochemistry P.N.V. and N.N.E.; quantum chemical calculations, D.V.K.; X-ray powder diffraction studies, A.S.G.; funding acquisition S.A.N. and I.L.E. All authors have read and agreed to the published version of the manuscript.

Funding: This study (synthesis of complex compounds, Single Crystal and Powder X-ray Diffraction, Magnetochemistry) was supported by the Russian Science Foundation (grant no. 19-13-00436). High-level

ab initio quantum chemical calculations have been supported by the state assignment of the Ministry of Science and Higher Education of the Russian Federation (no AAAA-A19-119092390079-8).

Acknowledgments: X-ray diffraction analysis, elemental and spectral analyzes, as well as magnetochemical studies were performed using the equipment at the Center for Collective Use of the Kurnakov Institute RAS, which operates with the support of the state assignment of the IGIC RAS in the field of fundamental scientific research.

Conflicts of Interest: The authors declare no conflict of interest.

References

1. Frost, J.M.; Harriman, K.; Murugesu, M. The rise of 3-d single-ion magnets in molecular magnetism: Towards materials from molecules? *Chem. Sci.* **2016**, *7*, 2470–2491. [[CrossRef](#)] [[PubMed](#)]
2. Murrie, M. Cobalt(II) single-molecule magnets. *Chem. Soc. Rev.* **2010**, *39*, 1986–1995. [[CrossRef](#)]
3. Tanaka, D.; Inose, T.; Tanaka, H.; Lee, S.; Ishikawa, N.; Ogawa, T. Proton-induced switching of the single molecule magnetic properties of a porphyrin based Tb^{III} double-decker complex. *Chem. Commun.* **2012**, *48*, 7796–7798. [[CrossRef](#)]
4. Horii, Y.; Horie, Y.; Katoh, K.; Breedlove, B.K.; Yamashita, M. Changing single-molecule magnet properties of a windmill-like distorted terbium(III) α -butoxy-substituted phthalocyaninato double-decker complex by protonation/deprotonation. *Inorg. Chem.* **2018**, *57*, 565–574. [[CrossRef](#)] [[PubMed](#)]
5. Liang, Z.; Damjanović, M.; Kamila, M.; Cosquer, G.; Breedlove, B.K.; Enders, M.; Yamashita, M. Proton Control of the lanthanoid single-ion magnet behavior of a double-decker complex with an indolenine-substituted annulene ligand. *Inorg. Chem.* **2017**, *56*, 6512–6521. [[CrossRef](#)] [[PubMed](#)]
6. Wang, H.-Y.; Cui, L.; Xie, J.-Z.; Leong, C.F.; D'Alessandro, D.M.; Zuo, J.-L. Functional coordination polymers based on redox-active tetrathiafulvalene and its derivatives. *Coord. Chem. Rev.* **2017**, *345*, 342–361. [[CrossRef](#)]
7. Faust, T.B.; D'Alessandro, D.M. Radicals in metal–organic frameworks. *RSC Adv.* **2014**, *4*, 17498–17512. [[CrossRef](#)]
8. Dorofeeva, V.N.; Pavlishchuk, A.V.; Kiskin, M.A.; Efimov, N.N.; Minin, V.V.; Lytvynenko, A.S.; Gavrilenko, K.S.; Kolotilov, S.V.; Novotortsev, V.M.; Eremenko, I.L. CoII Complexes with a tripyridine ligand, containing a 2,6-di-tert-butylphenolic fragment: synthesis, structure, and formation of stable radicals. *ACS Omega* **2019**, *4*, 203–213. [[CrossRef](#)]
9. Hu, S.; Lv, L.; Chen, S.; You, M.; Fu, Z. Zn-MOF-based photoswitchable dyad that exhibits photocontrolled luminescence. *Cryst. Growth Des.* **2016**, *16*, 6705–6708. [[CrossRef](#)]
10. Hong, J.; Zhuang, Y.; Ji, X.; Guo, X. A long-lived luminescence and EPR bimodal lanthanide-based probe for free radicals. *Analyst* **2011**, *136*, 2464–2470. [[CrossRef](#)]
11. Ovcharenko, V.I.; Romanenko, G.V.; Maryunina, K.Y.; Bogomyakov, A.S.; Gorelik, E.V. Thermally induced magnetic anomalies in solvates of the bis(hexafluoroacetylacetonate)copper(II) complex with pyrazolyl-substituted nitronyl nitroxide. *Inorg. Chem.* **2008**, *47*, 9537–9552. [[CrossRef](#)] [[PubMed](#)]
12. Fedin, M.; Veber, S.; Gromov, I.; Maryunina, K.; Fokin, S.; Romanenko, G.; Sagdeev, R.; Ovcharenko, V.; Bagryanskaya, E. Thermally induced spin transitions in nitroxide–copper(II)–nitroxide spin triads studied by EPR. *Inorg. Chem.* **2007**, *46*, 11405–11415. [[CrossRef](#)] [[PubMed](#)]
13. Fedushkin, I.L.; Skatova, A.A.; Chudakova, V.A.; Fukin, G.K. Four-step reduction of dpp-bian with sodium metal: crystal structures of the sodium salts of the mono-, di-, tri- and tetraanions of dpp-bian. *Angew. Chemie Int. Ed.* **2003**, *42*, 3294–3298. [[CrossRef](#)] [[PubMed](#)]
14. Sandl, S.; Maier, T.M.; van Leest, N.P.; Kröncke, S.; Chakraborty, U.; Demeshko, S.; Koszinowski, K.; de Bruin, B.; Meyer, F.; Bodensteiner, M.; et al. Cobalt-catalyzed hydrogenations via olefin cobaltate and hydride intermediates. *ACS Catal.* **2019**, *9*, 7596–7606. [[CrossRef](#)]
15. Lima, G.; Nunes, E.; Dantas, R.; Simone, C.; Meneghetti, M.; Meneghetti, S. Catalytic behaviors of Co^{II} and Mn^{II} compounds bearing α -diimine ligands for oxidative polymerization or drying oils. *J. Braz. Chem. Soc.* **2018**, *29*, 412–418. [[CrossRef](#)]
16. Fomenko, I.S.; Gushchin, A.L.; Shul'pina, L.S.; Ikonnikov, N.S.; Abramov, P.A.; Romashev, N.F.; Poryvaev, A.S.; Sheveleva, A.M.; Bogomyakov, A.S.; Shmelev, N.Y.; et al. New oxidovanadium(IV) complex with a BIAN ligand: synthesis, structure, redox properties and catalytic activity. *New J. Chem.* **2018**, *42*, 16200–16210. [[CrossRef](#)]

17. Singha Hazari, A.; Ray, R.; Hoque, M.A.; Lahiri, G.K. Electronic structure and multicatalytic features of redox-active bis(arylimino)acenaphthene (BIAN)-derived ruthenium complexes. *Inorg. Chem.* **2016**, *55*, 8160–8173. [[CrossRef](#)]
18. Kee, J.W.; Ng, Y.Y.; Kulkarni, S.A.; Muduli, S.K.; Xu, K.; Ganguly, R.; Lu, Y.; Hirao, H.; Soo, H.S. Development of bis(arylimino)acenaphthene (BIAN) copper complexes as visible light harvesters for potential photovoltaic applications. *Inorg. Chem. Front.* **2016**, *3*, 651–662. [[CrossRef](#)]
19. O'Brien, C.; Wong, M.Y.; Cordes, D.B.; Slawin, A.M.Z.; Zysman-Colman, E. Cationic platinum(II) complexes bearing aryl-BIAN ligands: synthesis and structural and optoelectronic characterization. *Organometallics* **2015**, *34*, 13–22. [[CrossRef](#)]
20. El-Ayaan, U.; Abdel-Aziz, A.A.-M. Synthesis, antimicrobial activity and molecular modeling of cobalt and nickel complexes containing the bulky ligand: bis[N-(2,6-diisopropylphenyl)imino]acenaphthene. *Eur. J. Med. Chem.* **2005**, *40*, 1214–1221. [[CrossRef](#)]
21. Pelties, S.; Maier, T.; Herrmann, D.; de Bruin, B.; Rebreyend, C.; Gärtner, S.; Shenderovich, I.G.; Wolf, R. Selective P₄ Activation by a highly reduced cobaltate: synthesis of dicobalt tetrakisphido complexes. *Chem.–A Eur. J.* **2017**, *23*, 6094–6102. [[CrossRef](#)]
22. Fedushkin, I.L.; Makarov, V.M.; Sokolov, V.G.; Fukin, G.K. Acenaphthene-1,2-diimine chromium complexes. *Dalton. Trans.* **2009**, 8047–8053. [[CrossRef](#)]
23. Fedushkin, I.L.; Makarov, V.M.; Sokolov, V.G.; Fukin, G.K.; Maslov, M.O.; Ketkov, S.Y. Compounds of chromium, titanium, and zirconium with different reduced forms of acenaphthene-1,2-diimine. *Russ. Chem. Bull.* **2014**, *63*, 870–882. [[CrossRef](#)]
24. Bendix, J.; Clark, K.M. Delocalization and valence tautomerism in vanadium tris(iminosemiquinone) complexes. *Angew. Chemie Int. Ed.* **2016**, *55*, 2748–2752. [[CrossRef](#)] [[PubMed](#)]
25. Morozov, A.G.; Fedushkin, I.L.; Irran, E.; Grohmann, A. Titanium(IV) complexes supported by a dianionic acenaphthenediimine ligand: X-ray and spectroscopic studies of the metal coordination sphere. *Inorg. Chem. Commun.* **2018**, *95*, 50–55. [[CrossRef](#)]
26. Abramov, P.A.; Dmitriev, A.A.; Kholin, K.V.; Gritsan, N.P.; Kadirov, M.K.; Gushchin, A.L.; Sokolov, M.N. Mechanistic study of the [(dpp-bian)Re(CO)₃Br] electrochemical reduction using in situ EPR spectroscopy and computational chemistry. *Electrochim. Acta* **2018**, *270*, 526–534. [[CrossRef](#)]
27. Romashev, N.F.; Gushchin, A.L.; Fomenko, I.S.; Abramov, P.A.; Mirzaeva, I.V.; Kompan'kov, N.B.; Kal'nyi, D.B.; Sokolov, M.N. A new organometallic rhodium(I) complex with dpp-bian ligand: Synthesis, structure and redox behaviour. *Polyhedron* **2019**, *173*, 114110. [[CrossRef](#)]
28. Gushchin, A.L.; Romashev, N.F.; Shmakova, A.A.; Abramov, P.A.; Ryzhikov, M.R.; Fomenko, I.S.; Sokolov, M.N. Novel redox active rhodium(III) complex with bis(arylimino)acenaphthene ligand: synthesis, structure and electrochemical studies. *Mendeleev Commun.* **2020**, *30*, 81–83. [[CrossRef](#)]
29. Saber, M.R.; Dunbar, K.R. Ligands effects on the magnetic anisotropy of tetrahedral cobalt complexes. *Chem. Commun.* **2014**, *50*, 12266–12269. [[CrossRef](#)]
30. Kansikas, J.; Leskelä, M.; Kenessey, G.; Werner, P.-E.; Liptay, G.; Balzarini, J.; Fransson, B.; Ragnarsson, U.; Francis, G. Preparation and characterization of 2,6- and 3,5-dimethylpyridine complexes of cobalt(II) halides; the crystal structure of di(2,6-dimethylpyridinium) tetrachlorocobaltate(II) and dichlorotetrakis(3,5-dimethylpyridine)cobalt(II). *Acta Chem. Scand.* **1994**, *48*, 951–959. [[CrossRef](#)]
31. Belén Lago, A.; Amoedo, A.; Carballo, R.; García-Martínez, E.; Vázquez-López, E.M. Metal coordination and in situ S–C bond cleavage of the bis(2-pyridylthio)methane ligand. *Dalton. Trans.* **2010**, *39*, 10076–10087. [[CrossRef](#)] [[PubMed](#)]
32. Stauber, J.M.; Wadler, A.L.; Moore, C.E.; Rheingold, A.L.; Figueroa, J.S. Coordination properties of 2,5-dimesitylpyridine: an encumbering and versatile ligand for transition-metal chemistry. *Inorg. Chem.* **2011**, *50*, 7309–7316. [[CrossRef](#)]
33. Smith, P.W.; Moore, C.E.; Rheingold, A.L.; Figueroa, J.S. Coordination and structural properties of encumbering 6-mesityl-2-picolinate complexes. *Dalton. Trans.* **2012**, *41*, 8031–8038. [[CrossRef](#)] [[PubMed](#)]
34. Smolko, L.; Černák, J.; Dušek, M.; Miklovič, J.; Titiš, J.; Boča, R. Three tetracoordinate Co(II) complexes [Co(biq)X₂] (X = Cl, Br, I) with easy-plane magnetic anisotropy as field-induced single-molecule magnets. *Dalt. Trans.* **2015**, *44*, 17565–17571. [[CrossRef](#)] [[PubMed](#)]
35. Smolko, L.; Černák, J.; Dušek, M.; Titiš, J.; Boča, R. Tetracoordinate Co(II) complexes containing bathocuproine and single molecule magnetism. *New J. Chem.* **2016**, *40*, 6593–6598. [[CrossRef](#)]

36. Smolko, L.; Černák, J.; Kuchár, J.; Rajnák, C.; Titiš, J.; Boča, R. Field-induced slow magnetic relaxation in mononuclear tetracoordinate cobalt(II) complexes containing a neocuproine ligand. *Eur. J. Inorg. Chem.* **2017**, *2017*, 3080–3086. [[CrossRef](#)]
37. Perry, D.L.; Phillips, S.L. *Handbook of Inorganic Compounds*; Taylor & Francis: Boca Raton, FL, USA, 1995; ISBN 9780849386718.
38. Paulovicova, A.; El-Ayaan, U.; Shibayama, K.; Morita, T.; Fukuda, Y. Mixed-ligand copper(II) complexes with the rigid bidentate bis(n-arylimino)acenaphthene ligand: Synthesis, spectroscopic-, and X-ray structural characterization. *Eur. J. Inorg. Chem.* **2001**, *2001*, 2641–2646. [[CrossRef](#)]
39. Rosa, V.; Carabineiro, S.A.; Aviles, T.; Gomes, P.T.; Welter, R.; Campos, J.M.; Ribeiro, M.R. Synthesis, characterization and solid state structures of α -diimine cobalt(II) complexes: Ethylene polymerization tests. *J. Organomet. Chem.* **2008**, *693*, 769–775. [[CrossRef](#)]
40. Fedushkin, I.L.; Skatova, A.A.; Yambulatov, D.S.; Cherkasov, A.V.; Demeshko, S.V. Europium complexes with 1,2-bis(arylimino)acenaphthenes: A search for redox isomers. *Russ. Chem. Bull.* **2015**, *64*, 38–43. [[CrossRef](#)]
41. Skatova, A.A.; Yambulatov, D.S.; Fedyushkin, I.L.; Baranov, E.V. Europium and ytterbium complexes with the redox active acenaphthene-1,2-diimine ligand. *Russ. J. Coord. Chem.* **2018**, *44*, 400–409. [[CrossRef](#)]
42. Rosa, V.; González, P.; Avilés, T.; Gomes, P.; Welter, R.; Rizzi, A.; Passeggi, M.; Brondino, C. Synthesis, solid-state structures, and EPR spectroscopic studies on polycrystalline and single-crystal samples of α -diimine cobalt(II) complexes. *Eur. J. Inorg. Chem.* **2006**, 4761–4769. [[CrossRef](#)]
43. Hantzsch, A. Solvation und Komplexbildung als Ursache des Farbenwechsels der Kobaltohaloide. *Zeitschrift für Anorg. und Allg. Chemie* **1927**, *159*, 273–303. [[CrossRef](#)]
44. Little, B.F.; Long, G.J. Moessbauer, electronic, and structural properties of several bis- and tetrakis(pyridine)iron(II) complexes. *Inorg. Chem.* **1978**, *17*, 3401–3413. [[CrossRef](#)]
45. Bushuev, M.B.; Krivopalov, V.P.; Peresyphkina, E.V.; Virovets, A.V.; Shvedenkov, Y.G.; Sheludyakova, L.A.; Semikolenova, N.V.; Zakharov, V.A.; Larionov, S.V. Complexes of copper(II) and cobalt(II) halides with 4-(3,5-dimethyl-1H-pyrazol-1-yl)-6-methyl-2-phenylpyrimidine: Synthesis, structures, and properties. *Russ. J. Coord. Chem.* **2009**, *35*, 597–608. [[CrossRef](#)]
46. Bushuev, M.B.; Virovets, A.V.; Peresyphkina, E.V.; Naumov, D.Y.; Potapov, A.S.; Khlebnikov, A.I.; Vasilevsky, S.F.; Lavrenova, L.G. Synthesis and structure of (bis(3,5-dimethyl-1H-pyrazol-1-yl)methane)diiodocobalt(II). *J. Struct. Chem.* **2005**, *46*, 1099–1103. [[CrossRef](#)]
47. El-Ayaan, U.; Paulovicova, A.; Yamada, S.; Fukuda, Y. The crystal structure of bis[n-(2,6-diisopropylphenyl)imino] acenaphthene and studies of its copper(I) and copper(II) complexes. *J. Coord. Chem.* **2003**, *56*, 373–381. [[CrossRef](#)]
48. Zhou, M.; Li, X.; Bu, D.; Lei, H. Synthesis, crystal structures and electrochemical properties of Co(II) and Mn(II) complexes with asymmetric bulky BIAN ligands. *Polyhedron* **2018**, *148*, 88–99. [[CrossRef](#)]
49. Alnajrani, M.N.; Alshimri, S.A.; Alsager, O.A. Alpha and beta diimine cobalt complexes in isoprene polymerization: a comparative study. *RSC Adv.* **2016**, *6*, 113803–113814. [[CrossRef](#)]
50. Supej, M.J.; Volkov, A.; Darko, L.; West, R.A.; Darmon, J.M.; Schulz, C.E.; Wheeler, K.A.; Hoyt, H.M. Aryl-substituted BIAN complexes of iron dibromide: Synthesis, X-ray and electronic structure, and catalytic hydrosilylation activity. *Polyhedron* **2016**, *114*, 403–414. [[CrossRef](#)]
51. Wekesa, F.S.; Arias-Ugarte, R.; Kong, L.; Sumner, Z.; McGovern, G.P.; Findlater, M. Iron-catalyzed hydrosilylation of aldehydes and ketones under solvent-free conditions. *Organometallics* **2015**, *34*, 5051–5056. [[CrossRef](#)]
52. Kahn, O. *Molecular Magnetism*; VCH Publ. Inc.: New York, NY, USA, 1993; p. 393.
53. Chilton, N.F.; Anderson, R.P.; Turner, L.D.; Soncini, A.; Murray, K.S. PHI: A powerful new program for the analysis of anisotropic monomeric and exchange-coupled polynuclear d- and f-block complexes. *J. Comput. Chem.* **2013**, *34*, 1164–1175. [[CrossRef](#)] [[PubMed](#)]
54. Pavlov, A.A.; Nelyubina, Y.V.; Kats, S.V.; Penkova, L.V.; Efimov, N.N.; Dmitrienko, A.O.; Vologzhanina, A.V.; Belov, A.S.; Voloshin, Y.Z.; Novikov, V.V. Polymorphism in a cobalt-based single-ion magnet tuning its barrier to magnetization relaxation. *J. Phys. Chem. Lett.* **2016**, *7*, 4111–4116. [[CrossRef](#)] [[PubMed](#)]
55. Ding, M.; Cutsail III, G.E.; Aravena, D.; Amoza, M.; Rouzières, M.; Dechambenoit, P.; Losovyj, Y.; Pink, M.; Ruiz, E.; Clérac, R.; et al. A low spin manganese(IV) nitride single molecule magnet. *Chem. Sci.* **2016**, *7*, 6132–6140. [[CrossRef](#)] [[PubMed](#)]

56. Polyizou, C.D.; Koumoussi, E.S.; Lada, Z.G.; Raptopoulou, C.P.; Psycharis, V.; Rouzières, M.; Tshipis, A.C.; Mathonière, C.; Clérac, R.; Perlepes, S.P. “Switching on” the single-molecule magnet properties within a series of dinuclear cobalt(III)–dysprosium(III) 2-pyridyloximate complexes. *Dalton. Trans.* **2017**, *46*, 14812–14825. [[CrossRef](#)]
57. Bilyachenko, A.N.; Yalymov, A.I.; Korlyukov, A.A.; Long, J.; Larionova, J.; Guari, Y.; Zubavichus, Y.V.; Trigub, A.L.; Shubina, E.S.; Eremenko, I.L.; et al. Heterometallic Na₆Co₃ phenylsilsesquioxane exhibiting slow dynamic behavior in its magnetization. *Chem.—A Eur. J.* **2015**, *21*, 18563–18565. [[CrossRef](#)] [[PubMed](#)]
58. Petrosyants, S.P.; Ilyukhin, A.B.; Efimov, N.N.; Gavrikov, A.V.; Novotortsev, V.M. Self-assembly and SMM properties of lanthanide cyanocobaltate chain complexes with terpyridine as blocking ligand. *Inorganica Chim. Acta* **2018**, *482*, 813–820. [[CrossRef](#)]
59. Mamontova, E.; Long, J.; Ferreira, A.S.R.; Botas, M.P.A.; Luneau, D.; Guari, Y.; Carlos, D.L.; Larionova, J. Magneto-luminescence correlation in the textbook Dysprosium(III) nitrate single-ion magnet. *Magnetochemistry* **2016**, *2*, 41. [[CrossRef](#)]
60. Gavrikov, A.V.; Koroteev, P.S.; Efimov, N.N.; Dobrokhotova, Z.V.; Ilyukhin, A.B.; Kostopoulos, A.K.; Ariciu, A.-M.; Novotortsev, V.M. Novel mononuclear and 1D-polymeric derivatives of lanthanides and (η^6 -benzoic acid)tricarbonylchromium: synthesis, structure and magnetism. *Dalton. Trans.* **2017**, *46*, 3369–3380. [[CrossRef](#)]
61. Jia, X.; Lin, H.; Huo, C.; Zhang, W.; Lü, J.; Yang, L.; Zhao, G.; Liu, Z.-L. Cation radical imino Diels–Alder reaction: A new approach for the synthesis of tetrahydroquinolines. *Synlett* **2003**, *2003*, 1707–1709. [[CrossRef](#)]
62. Lukoyanov, A.N.; Ulivanova, E.A.; Razborov, D.A.; Khrizanforova, V.V.; Budnikova, Y.H.; Makarov, S.G.; Rummyantsev, R.V.; Ketkov, S.Y.; Fedushkin, I.L. One-electron reduction of 2-Mono(2,6-diisopropylphenylimino)acenaphthene-1-one (dpp-mian). *Chem.—A Eur. J.* **2019**, *25*, 3858–3866. [[CrossRef](#)]
63. Beloglazkina, E.K.; Yudin, I.V.; Majouga, A.G.; Moiseeva, A.A.; Tursina, A.I.; Zyk, N.V. Synthesis and electrochemical study of 2-(2-pyridyl)benzothiazole complexes with transition metals (Co^{II}, Ni^{II}, and Cu^{II}). Molecular structure of aquabis [2-(2-pyridyl)benzothiazole]copper(II) diperchlorate. *Russ. Chem. Bull.* **2006**, *55*, 1803–1809. [[CrossRef](#)]
64. Khrizanforova, V.V.; Morozov, V.I.; Khrizanforov, M.N.; Lukoyanov, A.N.; Kataeva, O.N.; Fedushkin, I.L.; Budnikova, Y.H. Iron complexes of BIANs: Redox trends and electrocatalysis of hydrogen evolution. *Polyhedron* **2018**, *154*, 77–82. [[CrossRef](#)]
65. SMART (control) and SAINT (integration) Software; Version 5.0.; Madison Bruker AXS Inc. Bruker: Fitchburg, WI, USA, 1997.
66. Sheldrick, G.M. A short history of SHELX. *Acta Crystallogr. Sect. A* **2008**, *64*, 112–122. [[CrossRef](#)] [[PubMed](#)]
67. Roos, B.O.; Taylor, P.R.; Sigbahn, P.E.M. A complete active space SCF method (CASSCF) using a density matrix formulated super-CI approach. *Chem. Phys.* **1980**, *48*, 157–173. [[CrossRef](#)]
68. Siegbahn, P.; Heiberg, A.; Roos, B.; Levy, B. A comparison of the super-CI and the Newton–Raphson scheme in the complete active space SCF method. *Phys. Scr.* **1980**, *21*, 323–327. [[CrossRef](#)]
69. Siegbahn, P.E.M.; Almlöf, J.; Heiberg, A.; Roos, B.O. The complete active space SCF (CASSCF) method in a Newton–Raphson formulation with application to the HNO molecule. *J. Chem. Phys.* **1981**, *74*, 2384–2396. [[CrossRef](#)]
70. Angeli, C.; Cimiraglia, R.; Evangelisti, S.; Leininger, T.; Malrieu, J.-P. Introduction of n-electron valence states for multireference perturbation theory. *J. Chem. Phys.* **2001**, *114*, 10252–10264. [[CrossRef](#)]
71. Angeli, C.; Cimiraglia, R.; Malrieu, J.-P. n-electron valence state perturbation theory: A spinless formulation and an efficient implementation of the strongly contracted and of the partially contracted variants. *J. Chem. Phys.* **2002**, *117*, 9138–9153. [[CrossRef](#)]
72. Hess, B.A. Relativistic electronic-structure calculations employing a two-component no-pair formalism with external-field projection operators. *Phys. Rev. A* **1986**, *33*, 3742–3748. [[CrossRef](#)]
73. Pantazis, D.A.; Chen, X.-Y.; Landis, C.R.; Neese, F. All-electron scalar relativistic basis sets for third-row transition metal atoms. *J. Chem. Theory Comput.* **2008**, *4*, 908–919. [[CrossRef](#)] [[PubMed](#)]
74. Schäfer, A.; Huber, C.; Ahlrichs, R. Fully optimized contracted Gaussian basis sets of triple zeta valence quality for atoms Li to Kr. *J. Chem. Phys.* **1994**, *100*, 5829–5835. [[CrossRef](#)]
75. Schäfer, A.; Horn, H.; Ahlrichs, R. Fully optimized contracted Gaussian basis sets for atoms Li to Kr. *J. Chem. Phys.* **1992**, *97*, 2571–2577. [[CrossRef](#)]

76. Weigend, F.; Ahlrichs, R. Balanced basis sets of split valence, triple zeta valence and quadruple zeta valence quality for H to Rn: Design and assessment of accuracy. *Phys. Chem. Chem. Phys.* **2005**, *7*, 3297–3305. [[CrossRef](#)]
77. Neese, F. An improvement of the resolution of the identity approximation for the formation of the Coulomb matrix. *J. Comput. Chem.* **2003**, *24*, 1740–1747. [[CrossRef](#)]
78. Ganyushin, D.; Neese, F. First-principles calculations of zero-field splitting parameters. *J. Chem. Phys.* **2006**, *125*, 24103. [[CrossRef](#)]
79. Neese, F. Efficient and accurate approximations to the molecular spin-orbit coupling operator and their use in molecular g-tensor calculations. *J. Chem. Phys.* **2005**, *122*, 34107. [[CrossRef](#)]
80. Maurice, R.; Bastardis, R.; de Graaf, C.; Suaud, N.; Mallah, T.; Guihéry, N. Universal Theoretical Approach to Extract Anisotropic Spin Hamiltonians. *J. Chem. Theory Comput.* **2009**, *5*, 2977–2984. [[CrossRef](#)]
81. Neese, F. The ORCA program system. *WIREs Comput. Mol. Sci.* **2012**, *2*, 73–78. [[CrossRef](#)]

Sample Availability: Samples of the Cobalt(II) compounds are available from the authors.



© 2020 by the authors. Licensee MDPI, Basel, Switzerland. This article is an open access article distributed under the terms and conditions of the Creative Commons Attribution (CC BY) license (<http://creativecommons.org/licenses/by/4.0/>).